3D type I collagen environment leads up to a reassessment of the classification of human macrophage polarizations

Magali Court, Marie Malier, Arnaud Millet

3D type I collagen environment leads up to a reassessment of the classification of human macrophage polarizations

Magali COURT[1,2,#], Marie MALIER[1,2,#], Arnaud MILLET[1,2,3*]

1. Team Mechanobiology, Immunity and Cancer, Institute for Advanced Biosciences, Inserm U1209, CNRS UMR5309, La Tronche, France

2. Grenoble Alpes University, Grenoble, France

3. Research Department, University Hospital of Alpes, Grenoble, France

*Corresponding author:

Arnaud Millet MD PhD

Team Mechanobiology, Immunity and Cancer

Institute for Advanced Biosciences

Batiment Jean Roget 3ème étage

Faculté de Médecine de Grenoble

Domaine de la Merci

38700 La Tronche

France

e-mail: arnaud.millet@inserm.fr

Running Title: 3D environment and Macrophage Polarization

Words number: 3940

# These two authors contributed equally

Abstract

Macrophages have multiple roles in development, tissue homeostasis and repair and present a high degree of phenotypic plasticity embodied in the concept of polarization. One goal of macrophage biology field is to characterize these polarizations at the molecular level. To achieve this task, it is necessary to integrate how physical environment signals are interpreted by macrophages under immune stimulation. In this work, we study how a 3D scaffold obtained from polymerized fibrillar rat type I collagen modulates the polarizations of human macrophages and reveal that some traditionally used markers should be reassessed. We demonstrate that integrin β_2 is a regulator of STAT1 phosphorylation in response to IFNγ/LPS as well as responsible for the inhibition of ALOX15 expression in response to IL-4/IL-13 in 3D. Meanwhile, we also find that the CCL19/CCL20 ratio is reverted in 3D under IFNγ/LPS stimulation. 3D also induces the priming of the NLRP3 inflammasome resulting in an increased IL-1β and IL-6 secretion. These results give the molecular basis for assessing collagen induced immunomodulation of human macrophages in various physiological and pathological contexts such as cancer.

Keywords: Macrophages, Polarization, 3D culture, Collagen, Inflammation, Integrins, Inflammasome

1.Introduction

Macrophages are innate immune cells present in every tissues playing a critical role in homeostasis. As first line defenders, these cells are prone to modify their phenotype in response to their surrounding environment, sensing various signals and displaying a large panel of activation states in order to cope with various pathogens [1]. Even if it is now accepted that the spectrum of activation states of these cells is better viewed as a continuum, it is still interesting to understand how the environment is able to favour a pro-inflammatory (M1) or an anti-inflammatory (M2) phenotype which could represent the extremes of this spectrum [2]. M1 macrophages are specialized in the removal of pathogens and are classically obtained *in vitro* using a combination of IFN-γ and a Toll-like receptor (TLR) agonist like LPS (Lipopolysaccharide). M1 macrophages are associated with the production of reactive oxygen species and pro-inflammatory cytokines secretion like TNF-α, IL-6 or chemokines like CCL-20 [3,4]. M2 macrophages are obtained using a stimulation with IL-4 (that could be combined to IL-13) and are also called alternatively activated macrophages [5]. These cells are described as anti-inflammatory and seem to participate to wound healing. This polarization is notably associated with the membrane expression of the mannose receptor also named CD206 [5]. Modifying the polarization of macrophages has emerged as a new therapeutical approach in inflammatory diseases and in cancer [2]. This goal, in order to be attained, needs that macrophage polarizations are properly defined and the influence of their cellular environment clarified. Even if it is possible to modify the activation state of macrophages using various chemical signals, it has been recently recognized that macrophages are also sensitive to their physical environment [6]. The growing interest of biomaterials in the medical field has revealed that these tools will interact mechanically and chemically with the host in various ways in a time dependent manner. The field of tissue engineering and regenerative medicine is devoted to the understanding of how physico-chemical characteristics of biomaterials will influence the success of their implantation. Macrophages are involved during all phases of host response toward

biomaterials, so their ability to adapt to this new environment is of outstanding interest. The understanding of how macrophages respond to biomaterials opens the way to design of materials that specifically target these cells, and obtain by the way a scaffold-induced immunomodulation [7,8]. This approach is particularly promising in the field of regenerative medicine [9]. More generally the question of how a three dimensional environment impacts immune cell functions has been recently recognized as a key element in our understanding of the tumour microenvironment. In this context, biomaterials offer a clear opportunity to decipher molecular and cellular processes involved in the macrophage-extracellular matrix-cancerous cells interactions [10].

In order to address that question, it is mandatory to understand how the three dimensional environment could modify the molecular signature of macrophages polarizations. Previous studies have demonstrated that macrophages are able to sense their physical environment. Patterned substrates modifying the elongation of mice macrophages was able to regulate the expression of arginase-1 and iNOS in M2 and M1 bone marrow derived macrophages respectively [11]. The elasticity of a substrate is another physical parameter that has been studied. Notably two dimensional functionalized gels of varying stiffness have revealed that macrophage present a mechanically controlled response to TLR agonists [12–15]. Other works have tried to understand how extracellular matrix properties impact macrophages polarization. A surface of collagen I functionalized with sulphated hyaluronan was associated with a downregulation of pro-inflammatory cytokines produced by GM-CSF differentiated human macrophages [16]. In order to mimic more closely the cellular environment, 3D scaffolds are used to reconstitute a structure similar to the extracellular matrix found *in vivo*. When 3D collagen networks functionalized by glycosaminoglycan are used the IL-10/IL12p40 ratio could be modified in human macrophages compared to 2D [17]. 3D fibrillary matrices from naturally derived collagen based networks are particularly interesting as they reconstitute the microstructure of the *in vivo* extracellular matrix [18]. We use in this study 3D collagen gels compared to 2D collagen coated surfaces to perform a differentiation of

human monocytes toward macrophages and secondarily polarize these macrophages toward a M1 (LPS+IFN-γ) and a M2 (IL-4+IL-13) phenotype. In order to obtain the molecular signature of these macrophages we used a whole transcriptome shotgun sequencing (RNAseq) analysis and a label-free quantification of protein expression to highlight genes and proteins specifically modulated by the 3D environment leading to a reappraisal of the M1/M2 dichotomy in human macrophages.

2. Materials and Methods

2.1 Ethical statements

Human blood samples from healthy de-identified donors are obtained from EFS (French national blood service) as part of an authorized protocol (CODECOH DC-2018–3114). Donors gave signed consent for use of their blood in this exploratory study.

2.2 Cell culture

Peripheral blood mononuclear cells (PBMC) are obtained from whole blood (leukocyte reduction system cones) by density gradient centrifugation (Histopaque 1077, Merck Millipore, Burlington, Massachusetts, USA). Monocytes are isolated from PBMCs using CD14 magnetic beads (Miltenyi Biotec, Paris, France) according to the manufacturer's instructions. Purity is assessed by flow cytometry for $CD14^{hi}CD45^{hi}$ cells and found to be > 96%. Monocytes are cultured in RPMI-Glutamax (Life Technologies, Courtaboeuf, France) supplemented with 10% human serum AB (Merck Millipore) and differentiation is induced by M-CSF (25 ng/ml) over 6 days at 10^6 cells per well in 12 wells culture plates. 3D conditions were obtained by seeding the monocytes on the top of gels which invade the gel during differentiation. Polarization is subsequently obtained using the same concentration of M-CSF and adding specific stimulations for a total of 48 h. Polarization states are induced as follows: M1 macrophages IFNγ 10 ng/ml + LPS 1 ng/ml and M2 macrophages IL-4 20 ng/ml + IL-13 20 ng/ml. Cells are counted in a Malassez chamber, using trypan blue exclusion to identify live cells. All cytokines and growth factors are purchased from Miltenyi Biotec,

134 France. LPS serogroup 0111 B4 is purchased from Calbiochem (Merck Millipore). The
135 NLRP3 specific inhibitor MCC950 and ATP are purchased from Invivogen (Toulouse,
136 France).

137 *2.3 Collagen scaffold*

138 3D scaffolds are generated with Collagen I from Rat tail (Life technologies). Gelation is
139 performed according to manufacturer recommendations. Briefly, collagen is diluted to 2
140 mg/mL in PBS (Life Technologies) and pH at 7.0 is obtained using sterile NaOH (Merck
141 Millipore). Collagen is then incubated at 37°C in a humidified incubator for 40 minutes. Gels
142 are gently rinsed with culture medium for 15 minutes before cell seeding. 2D coating is
143 obtained using a solution of collagen at 50 µg/mL in 20 mM acetic acid (Merck Millipore) and
144 incubated at room temperature for one hour. The resulting surface concentration of collagen
145 is 5 µg/cm². Cells were harvested from collagen scaffold using collagenase (Life
146 Technologies) in HBSS containing calcium and magnesium (Life Technologies).

147 *2.4 Chemokine arrays and ELISA*

148 Chemokines are analysed using a Human Chemokine assay kit (R&D systems, Lille,
149 France) according to manufacturer recommendations. Signals from membranes are
150 analysed with a ChemiDoc Analysis System (BioRad, Marnes la coquette, France). Data are
151 quantified using the Fiji Software (1.51n, National Institutes of Health, USA). Human TNFα,
152 IL-6, IL-1β and CCL19 ELISA are purchased from Invitrogen (Carlsbad, California, USA).
153 Human CCL20 ELISA is purchased from Thermoscientific Pierce (Life Technologies). The
154 assays are performed according to manufacturer instructions.

155 *2.5 RNA sequencing*

156 RNA is isolated from 10^6 cells for each polarization using the MirVana isolation kit™
157 (Ambion, Applied Biosystems, Foster City, California, USA). Long RNA and small RNA
158 (<200 bp) are collected separately. RNA quality and quantity are assessed by performing an
159 Agilent Eukaryote Total RNA Nano assay in a 2100 Bioanalyzer (Agilent Technologies,

160 Santa Clara, California, USA). Libraries are prepared with TruSeq Stranded mRNA kit
161 protocol according to supplier recommendations. Briefly the key stages of this protocol are
162 successively, the purification of PolyA containing mRNA molecules using poly-T oligo
163 attached to magnetic beads from 1µg total RNA, a fragmentation using divalent cations
164 under elevated temperature to obtain approximately 300bp pieces, double strand cDNA
165 synthesis and finally Illumina adapters ligation and cDNA library amplification by PCR for
166 sequencing. Sequencing is then carried out on paired-end 75 bp of Illumina HiSeq4000.
167 Quality of reads is assessed for each sample using FastQC
168 (http://www.bioinformatics.babraham.ac.uk/projects/fastqc/). Fastq files are aligned to the
169 reference human genome hg19/GRCh37 with tophat2 (-p 16 -r 150 -g 2 --library-type fr-
170 firststrand) [19]. We remove reads mapping to multiple locations. We use HTSeq [20] to
171 obtain the number of reads associated to each gene in the Gencode v24lift37. We use the
172 Bioconductor *DESeq* package [21] to import raw HTSeq counts for each sample into R
173 statistical software and extract the count matrix. After normalizing for library size factors, we
174 normalize the count matrix by the coding length of genes to compute FPKM scores (number
175 of fragments per kilobase of exon model and millions of mapped reads). Bigwig visualization
176 files are generated using the bam2wig python script [22].FPKM data were further analyzed
177 using JMP software (v.13.0.0, SAS Institute Inc., Cary, North Carolina, USA).

178 *2.6 Proteomics*

179 Cells are directly lysed in Laemmli buffer and prepared and analysed as previously
180 described [23]. Briefly, the protein equivalent of 300 000 cells for each sample is loaded on
181 NuPAGE Bis-Tris 4–12% acrylamide gels (Life Technologies). Electrophoretic migration is
182 controlled to allow each protein sample to be split into six gel bands. Gels are stained with
183 R-250 Coomassie blue (Bio-Rad) before excising protein bands. Gel slices are washed then
184 dehydrated with 100% acetonitrile (Merck Millipore), incubated with 10 mM DTT
185 (Dithiothreitol, Merck Millipore) in 25 mM ammonium bicarbonate (Merck Millipore) for 45 min
186 at 56 °C, followed by 55 mM iodoacetamide (Merck Millipore) in 25 mM ammonium

bicarbonate for 35 min in the dark. Alkylation is stopped by adding 10 mM DTT in 25 mM ammonium bicarbonate. Proteins are digested overnight at 37 °C with Trypsin/Lys-C Mix (Promega, Charbonnières, France) according to manufacturer's instructions. After extraction fractions are pooled, dried and stored at -80 °C until further analysis. The dried extracted peptides are resuspended and analyzed by online nano-LC (Ultimate 3000, Thermo Scientific) directly linked to an impact IITM Hybrid Quadrupole Timeof- Flight (QTOF) instrument fitted with a CaptiveSpray ion source (Bruker Daltonics, Bremen, Germany). All data are analyzed using Max- Quant software (version 1.5.2.8) and the Andromeda search engine [24,25]. The false discovery rate (FDR) is set to 1% for both proteins and peptides, and a minimum length of seven amino acids was set. MaxQuant scores peptide identifications based on a search with an initial permissible mass deviation for the precursor ion of up to 0.07 Da after time-dependent recalibration of the precursor masses. Fragment mass deviation is allowed up to 40 ppm. The Andromeda search engine is used to match MS/MS spectra against the Uniprot human database (https://www.uniprot.org/). Enzyme specificity is set as C-terminal to Arg and Lys, cleavage at proline bonds and a maximum of two missed cleavages are allowed. Carbamidomethylation of cysteine is selected as a fixed modification, whereas N-terminal protein acetylation and methionine oxidation are selected as variable modifications. The "match between runs" feature of MaxQuant is used to transfer identification information to other LC-MS/MS runs based on ion masses and retention times (maximum deviation 0.7 min); this feature is also used in quantification experiments. Quantifications are performed using the label-free algorithms [24]. A minimum peptide ratio counts of two and at least one "razor peptide" are required for quantification. The LFQ metric is used to perform relative quantification between proteins identified in different biological conditions, protein intensities are normalized based on the MaxQuant "protein group.txt" output (reflecting a normalized protein quantity deduced from all peptide intensity values). Potential contaminants and reverse proteins are strictly excluded from further analysis. Three analytical replicates from two independent biological samples (donors) are analyzed for each polarization in the 2D and 3D conditions. Missing values are deduced from a normal

distribution (width: 0.3; down shift: 1.8) using the Perseus (version 1.5.5.3) post data acquisition package contained in MaxQuant (www.maxquant.org). Data are further analyzed using JMP software (v.13.0.0, SAS Institute Inc.). Proteins are classed according to the paired Welch *t* test difference (difference between the mean value for triplicate MS/MS analyses for the two conditions compared), and the median fold-change between the two conditions compared.

2.7 Atomic Force Microscopy

Atomic force microscopy is performed in PBS at room temperature in indentation-force volume mode using a Flex-ANA system on fresh samples (Nanosurf, Liestal, Switzerland). Borosilicate beads (radius 5µm) mounted on QP-SCONT cantilevers (NanoAndMore, Wetzlar, Germany) are used. The spring constant is determined by thermal tuning [26]. The force setpoint is fixed at 3 nN. Each sample is mapped with at least 3 maps with 20x20 force volume curves. Elasticity is determined from the retraction curve using the AtomicJ software [27]. We use a Hertz-model to relate the force and the indentation as adhesion is negligible compared to our force setpoint and indentation far less than our tip radius. In this model, the force F is related to the indentation δ and the Young's modulus E by the following relation

$$F = \frac{4\sqrt{R}\,E}{3(1-\upsilon^2)}\delta^{\frac{3}{2}}$$

Where R is the radius of the tip and υ the Poisson ratio taken at 0.5 here.

2.8 Immunoblots

Cell lysates from HMDM are prepared in RIPA with protease inhibitors (PMSF, Pepstatine A, Leupeptin) and phosphatase inhibitors (Orthovanadate, Betaglycerophosphate, NaF), all products purchased from Merck Millipore. Total amount of proteins is determined by BCA Protein Assay kit (Pierce-Life Technologies). A volume corresponding to 15 µg is deposited and run on SDS-polyacrylamide gels according to standard SDS-PAGE protocols. The primary antibodies used are anti-TGM2 (MA5-12739; ThermoFischer, Rockford, Illinois,

USA), anti-ALOX15 (ab119774; Abcam, Cambridge, UK), anti-STAT1α/β (sc-464; Santa Cruz, Dallas, Texas, USA), anti-pSTAT1ser727 (sc-16570, Santa Cruz), anti-STAT6 (PA5-34814, Life Technologies), anti-pSTAT6Tyr647 (sc-136019, Santa Cruz), anti-CD206 (sc-376232, Santa Cruz), anti-CASP1(MAB6215, R&D systems) and anti β-actin (A2228, Merck Millipore) as loading control. Signal is detected by chemoluminiscence (Chemi-Doc Imaging System, Bio-Rad) after incubation with horseradish peroxide-conjugated secondary antibody (Jackson Immunoresearch, Ely, UK).

2.9 Integrin receptor blocking

Human monocytes are incubated with 10 µg/mL of various anti-integrin antibodies: anti CD11a (ITGAL; clone HI111 BioLegend, London, UK), anti CD11b (ITGAM; clone ICRF44 BioLegend), anti CD11c (ITGAX; clone 3.9 BioLegend), anti CD18 (ITGB2 integrin β_2; clone TS1/18 BioLegend), anti CD29 (ITGB1 integrin β_1; clone P4C1 Merck Millipore), anti-integrin β_3 (ITGB3; clone 2C9 Invitrogen) and integrin α_2(ITGA2; clone P1E Merck Millipore) for 6 days. The same antibodies are added again during polarisation for the next 48h.

2.10 Confocal imaging of 3D macrophages

Macrophages in 3D gels were fixed with paraformaldehyde 4% for 15 minutes. Cells were permeabilized by Triton X-100 at 0.5% for 5 minutes. Then actin cytoskeleton was stained using phalloidin-alexa 488 (Invitrogen) and nucleus stained with Hoechst (Life Technologies). Confocal imaging experiments were performed using a LSM710 NLO (Carl Zeiss) laser scanning microscope based on the inverted motorized stand (AxioObserver). The Hoechst and Alexa488 excitations were provided by 405 nm DPSS and 488 nm Ar lasers and descanned detection was in the ranges 410-490 and 500–550 nm respectively. The pinhole was closed to 1 Airy Unit. The long working distance water immersion objective 40x/1.0 W LD Apochromat was used to image cells at > 700 µm depth. The absence of correction for the coverslip thickness was responsible for the pronounced spherical

aberration that reduced the sensitivity and axial resolution. Z-stack over 350 µm was imaged with the step of 2 µm, the lateral pixel size was 413 nm.

2.11 Statistical Analysis

All statistical tests are done using GraphPad Prism (v7 GraphPad Prism Software, Inc, San Diego, California, USA). Multiple comparisons have been done using a paired Tukey's multiple comparison test when all conditions were compared or a paired Dunnett's multiple comparison test when comparisons are performed toward a control condition. Proteomic and transcriptomic analyses have been performed with two paired conditions using a Welch t test. We have indicated in each figure legend the appropriate test used. The threshold for statistical significance is set to a p value < 0.05.

3. Results

3.1 The human macrophage M1/M2 dichotomy is impacted by the physical environment

We use two different polarizations named subsequently M1 and M2 corresponding to stimulation with IFNγ/LPS and IL4/IL13 respectively after a differentiation with M-CSF from human circulating monocytes. In order to study the influence of the physical environment on the assessment of the differences between these two polarisations states, we conduct the differentiation process on 2D collagen coated surfaces and 3D collagen gels (Figure 1A). On 2D collagen coated surfaces macrophages do not present significant morphological differences between the two polarizations (Figure 1B). In 3D cells are typically smaller even if some M1 still present an elongated phenotype (Figure 1B) and are distributed in a depth of 350 µm in the gel (Supplemental Figure 1). In order to determine the impact of the environment on human macrophage polarisation states, we used a transcriptomic approach. The principal component analysis (PCA) of RNAseq data reveals that, as expected, the M1 and M2 activation states in 2D and in 3D can be clearly separated with a first principal component covering 43.8% of variations (Figure 1C). Furthermore, each polarization under a 3D environment is distinguishable from its 2D counterpart, associated with the second

principal component covering 21.5% of variations (Figure 1C). In order to describe what are the differentially expressed genes associated with each polarization, we compared the expression of genes involved in the M1/M2 dichotomy in the context of a 2D and a 3D environment (Figure 1D). Using a fold change (FC) greater or equal to 2, we find 552 upregulated genes in M1 and 335 genes upregulated in M2 for the 2D environment. For the 3D environment, we find 501 and 310 upregulated genes for M1 and M2 respectively. Our analysis reveals that 548 genes are differentially expressed in M1 macrophages in both environments, we also find 327 of common genes for M2 macrophages (Supplemental Table 1 & 2). Even if the categorization as M1 and M2 is mainly valid in the transfer from 2D to 3D as it is illustrated by the large number of genes upregulated in a particular polarization shared between 2D and 3D, we are able to obtain specific molecular signatures for each conditions (Supplemental Figure 2 A & B). We then study the consequences of these differences and the molecular pathways implicated.

3.2 The 3D environment amplifies the macrophage response to IFNγ mediated by the phosphorylation of the transcription factor STAT1 in an integrin β2 dependant mechanism

STAT1 is the main transcription factor involved in IFNγ response in macrophages [2,4], which through its phosphorylation is relocated to the nucleus in order to control the expression of IFNγ dependent genes [28]. We have found that STAT1 isoforms α and β are mainly present in M1 macrophages, confirming our previous published results that STAT1 expression is regulated under stimulation in addition to the control of its phosphorylation [23] contrary to what is generally found for other STAT molecules for which the main level of control concerns phosphorylation alone [29]. Meanwhile, we found a significant increase of the level of phosphorylation at serine 727 (S727) for macrophages in 3D (Figure 2A). We then seek to understand if this activation is related to a direct integrin-mediated interaction with collagen fibers. We cultivate our macrophages with various blocking antibodies against known expressed integrins at the human macrophage membrane: integrin α_L (CD11a, ITGAL), integrin α_M (CD11b, ITGAM), integrin α_X (CD11c, ITGAX), integrin β_2 (CD18,

ITGB2), integrin β_1 (CD29, ITGB1), integrin α_2 (ITGA2) and anti-integrin β_3 (ITGB3). These integrins are found to be expressed in every conditions without modulation according to the 2D/3D environment except for integrin β_3 which was found to be mainly expressed in 3D M1 macrophages (Supplemental Figure 3). Indeed, we found that the blocking of integrin β_2 was able to decrease significantly the expression of $pSTAT1^{ser727}$ (Figure 2B upper panel) without affecting the level of expression of STAT1α/β (Figure 2B, lower panel). Recently the role of integrins in the phosphorylation of STAT1 has been similarly reported in IFNγ activated T lymphocytes [30].

3.3 IL-4/IL-13 stimulation is associated with an enhancement of the phosphorylation of STAT6 and a downregulation of ALOX15 through integrin β_2 mediated signalling in 3D

IL-4/IL-13 stimulation leads to the phosphorylation of the transcription factor STAT6 [2]. We found that the phosphorylation of tyrosine 641 (Y641) site is significantly increased in 3D M2 macrophages (Figure 3A). To determine if this increase in STAT transcription factors phosphorylation in collagen scaffolds is functionally relevant, we performed a label free quantification proteomic approach to find differential expression of specific proteins in macrophages in 2D and 3D. We found that two known specific M2 markers, the arachidonate lipo-oxygenase (ALOX15) and the transglutaminase 2 (TGM2) were differentially expressed between 2D and 3D (Supplemental Figure 4). We confirm this pattern of expression by immunoblots. ALOX15 expression is downregulated in 3D contrary to TGM2 which presents an up-regulation (Figure 3B). The downregulation of ALOX15 is found to be transcriptionally controlled as it is demonstrated by its reduced mRNA level in 3D compared to 2D (Figure 3C), despite the fact that pSTAT6 is one of the transcription factor that control its expression [31]. To explain this pSTAT6 independent regulation, we then study if integrins are implicated in this expression and find that integrin β_2 when blocked by a specific antibody restores ALOX15 level comparable to 2D controls (Figure 3D). Other M2 expressed proteins like CD206 or TGM2 are not significantly modulated by the blocking of integrins. We also find that the increase of phosphorylation of STAT6 is not mediated by

integrins β_2, β_1, β_3, α_L, α_M, α_X or α_2 (Supplemental Figure 4). The activation of integrin β_2 has been reported in monocytes as a potent inhibitor of the expression of ALOX15 under IL-4 or IL-13 stimulation [32].

3.4 The 3D environment abrogates the differential expression of class II histocompatibility complex proteins between M1 and M2 macrophages

The Gene Ontology (GO) analysis of genes characterizing M2 macrophages reveals specific GO-Terms differentiating 2D and 3D environment. We find that numerous genes implicated in the processing and presentation of antigen via the major histocompatibility complex II are specific to M2 macrophages in a 2D environment (Figure 4A). We consequently analyse the expression of class I and class II HLA molecules and find that M1 macrophages, irrespective of their 2D or 3D condition, are associated with an overexpression of class I HLA genes (*HLA-A*, *HLA-B, HLA-C, HLA-E, HLA-F*) (Figure 4B). We obtain the same pattern at the protein level using our proteomic quantification approach which shows that HLA-A, B and C are upregulated in M1 macrophages irrespective of the 2D or 3D environment (Figure 4C). Following the GO-term analysis, we find that class II HLA molecules do not follow that pattern of expression and are found upregulated in M2 macrophages in 2D. Interestingly, this differential expression of genes (Figure 4B) and proteins (Figure 4C) of the class II HLA system is no longer found in 3D.

3.5 The secretome of IFNγ/LPS stimulated macrophages in 3D is characterized by a IL-6 integrin dependent increased release and an inversed CCL19/CCL20 ratio

The secretome of macrophages is a powerful tool used to distinguish M1 and M2 in humans. Using our RNAseq analysis we find various cytokines and chemokines genes that are regulated according to a peculiar polarization (Figure 5A). We find that *CCL2*, *CCL3*, *CCL7*, *CCL8*, *CCL15*, *CXCL2*, *CXCL3*, *CXCL5*, *CXCL8*, *CXCL9* and TNF-α are M1 specific markers and *CCL13*, *CCL18* and *CCL26* M2 markers. These markers reach the following selection criteria fold change >4 and p-adjusted value <0.05 in 2D and 3D (Figure 5A).

Meanwhile, we find cytokines, chemokines and some receptors which are significantly differentially expressed but only in one physical environment. This is notably the case for *CCL19* and *CCL20*. We find that these two M1 chemokines present an inverted expression in 2D and 3D environment. CCL19 appears downregulated transcriptionally in 3D, and we effectively confirm that the protein is significantly more secreted in 2D macrophages when stimulated by IFNγ/LPS (Figure 5A, 5B and 5C, Supplemental Figure 6A). This regulation of the expression of CCL19 is followed by its receptor CCR7 (Figure 5A). We then find that CCL20 presents the exact opposite behaviour (Figure 5A, 5B and 5C, Supplemental Figure 6A). The CCL19 downregulation is not related to an integrin dependent mechanism (Supplemental Figure 6B), as the specific blocking of integrins does not restore its level of secretion found in 2D. In contrast, the IL-6 cytokine is increasingly released in M1 3D macrophages and this secretion could be blocked by targeting specifically integrins β_2 but also α_2, β_1 and β_3 (Figure 5D). The TNF-α secretion is, by contrast, not modulated by the 3D environment and blocking antibodies against integrins do not modulate its release (Figure 5E). Even if integrin β_3 is not believed to interact with collagen, it has been shown to be an agonistic receptor for IL-1β signalling [33] and IL-1β is known to induce the secretion of IL-6 [34]. As M1 3D macrophages are associated specifically with an increased IL-1β secretion (Figure 5A, Figure 6A ,6B, 6C), we propose that integrin β_3 is involved in IL-6 secretion in 3D through its interaction with IL-1β.

3.6 The NLRP3 inflammasome is pre-activated in 3D and IFNγ/LPS polarized macrophages in 3D present an increased IL-1β secretion

Analysis of the specific cytokines of M1 in 3D reveals a IL-1 type cytokine signature. Indeed, the mRNA of *CASP1* and *IL1B* are increased in 3D under the IFNγ/LPS stimulation (Figure 6A). We confirm that M1 3D macrophage do secrete more functional IL-1β than their 2D counterpart (Figure 6B). 3D macrophages prior to polarization do not secrete significantly detectable levels of IL-1β (data not shown). We also find that expression of pro-CASP1 at the protein level in 3D IFNγ/LPS stimulated macrophages is strongly increased compared to

2D by immunoblotting (Figure 6C). Because IL-1β secretion is mainly obtained by conversion of pro-CASP1 in CASP1 by the NLRP3 inflammasome molecular complex and secondarily the cleavage of pro-IL-1β by the activated CASP1, we hypothesize that IL-1β secretion in 3D M1 macrophages is NLRP3-mediated. Using a specific inhibitor (MCC950) of the NLRP3 inflammasome, we demonstrate the implication of this inflammasome in the specific M1 3D secretome signature (Figure 6D). To demonstrate that the NLRP3 inflammasome of macrophages is prone to present a stronger activation in 3D, we used LPS exposed macrophages secondarily stimulated by ATP (a potent driver of intracellular entry of K^+) and we demonstrate that the NLPR3 inflammasome is strongly activated in 3D compared to 2D (Figure 6E). This NLRP3 inflammasome activation phenotype in 3D is not under the control of an integrin-dependent mechanism as blocking of the integrins by specific antibodies does not modify the IL-1β secretion (Figure 6F).

4. Discussion

Macrophage polarizations, which are also referred to as activation states, have emerged as fundamental criteria to characterize innate immune responses in various pathological contexts [35]. Recently a joint effort has been made by macrophage's biologists to clarify the nomenclature and the understanding of polarization states [4]. As polarizations translate the fact that macrophages are able to display a large panel of phenotypes depending on the various signals they encounter, this task is notoriously difficult. The recognition that polarization is related to the activation of these cells at a particular point in space and time, has led to the recognition of the importance of cellular response to growth factors, cytokines or TLR agonists [35]. But macrophages are also able to sense other extracellular signals and it is now recognized that these cells present a strong sensitivity to their physical and mechanical environment [6]. We have designed the present study to answer the question of how polarizations in human macrophages are modulated by a 3D collagen scaffold. We use a high throughput transcriptomic and proteomic approach to obtain a molecular signature of two polarizations (M1 and M2) in a 3D context compare to its 2D counterpart. We find that in

order to properly characterize these polarizations, we need to know in which physical context the cells are (Figure 1). We first study how transcription factors associated with these two polarisations are impacted and find that their response (phosphorylation state) is increased. For IFNγ/LPS stimulated macrophages (M1) we find that the phosphorylation of the transcription factor STAT1 is mediated by integrin β_2 in a 3D collagen gel. Indeed, a blocking antibody directed against this integrin is able to normalized the response of $pSTAT1^{ser727}$ compared to what is observed in 2D (Figure 2). Previous works have reported that macrophages seem to interact with collagen through integrin β_1 but denatured collagen was used as adhesion substratum [36]. THP1 monocytic cell line is also believed to interact with fibronectin [37] or gelatin methacryloyl [38] through integrin β_1. Despite these results, when native collagen is used human monocytes interact with collagen mainly using integrin β_2 [39].

STAT6 transcription factor is phosphorylated under IL-4 or IL-13 stimulation. We find that 3D macrophages present an increased response to IL-4/IL-13 as demonstrated by the phosphorylation of tyrosine 641 (Y641). This response does not seem to be related to integrins signalling (Supplemental Figure 5). We then find that known M2 markers seem to present differential expression in 2D and 3D. ALOX15 which is a lipoxygenase has its expression abolished in 3D despite the fact that IL-4/IL-13 are strong inducers of its expression in 2D. We find that integrin β_2 is the main molecular culprit of this downregulation of ALOX15 expression (Figure 3). Because ALOX15 is involved in many inflammatory response of macrophages such as production of arachidonic acid catabolites, resolvins, protectins and clearance of apopotic cells [40], the 3D environment appears as a potent immune-modulator. ALOX15 is also believed to be a specific M2 marker [4] which could be dampened by integrin β_2 activation even if respective to their pSTAT6, CD206 and TGM2 [41] status these macrophages are classified as M2 (Figure 3D). These modifications could also impact other immune functions of macrophages, we find that the expression of class II HLA molecules that are used to characterize the state of activation present a different expression pattern in 2D and 3D. These molecules are found to be differentially expressed in

2D notably in response to LPS and we confirm that IL4/IL13 macrophages present a stronger expression of these molecules. This differential expression is not conserved in 3D where M1 and M2 macrophages are indistinguishable according to HLA class II expression levels. That is not the case for class I HLA molecules that conserve in 3D the differential expression of these molecules in M1 macrophages expressing a higher level than their M2 counterparts (Figure 4).

The secretome of macrophages is largely used to assess their polarization. It has been reported that physical parameters of the physical environment, like elasticity, could influence the response of macrophages to TLR agonist. Human GM-CSF differentiated macrophages in 3D fibrillar matrices of collagen and glycosaminoglycan display a lower response to LPS concerning their ability to secrete IL-10, IL-12 and TNF-α compared to 2D macrophages [17]. Mechanical elasticity has been mainly studied in 2D systems with functionalized polyacrylamide gels and contradictory results have been reported due to variety of chemistry used [42] and the variety of monocytic cell lines used. RAW and U937 cultured on polylysine functionalized 2D gels are prone to increase TNF-α secretion in response to LPS in softer gels [14] whereas mice bone marrow derived macrophage gave the opposite result on collagen coated gels [15]. PEG functionalized gels were even associated with a bimodal secretion pattern of IL-8 in THP1 cells [13]. Despite the variety of systems used, the main conclusion that could be drawn from these studies is the necessity to take into account the physical environment in order to appreciate macrophage response to TLR agonists. These studies also revealed the role of elasticity in macrophage response to immune stimuli like TLR agonists but it should be stressed that in order to obtain a differing response a large range of values of Young's modulus was required.

Because M1 macrophages are associated with the expression of metallo-proteinases like *MMP9*, *MMP14*, *MMP25* (Supplemental Table 1) which could degrade the extracellular matrix, especially collagen through their activation of MMP2 and correspondingly because M2 macrophages are associated with the expression of TGM2 (Supplemental Table 2) which

is able to crosslink collagen fibres [43], we verified if our human M1 or M2 macrophages are prone to modify the elasticity of their surrounding environment in 3D. We used an indentation type atomic force microscopy analysis to measure Young modulus of collagen gels containing M1 and M2 macrophages. We find no significant differences between the two types of macrophages advocating that in our setting the differences between M1 and M2 in 3D are not related to a differential elasticity between the two surrounding physical environments (Supplemental Figure 7).

In our study, we find that the response of macrophages to IFNγ/LPS is more complex than previously thought. We notably find that no general inflammatory or anti-inflammatory pattern could be drawn when 2D and 3D are compared. Some studied chemokines present an unmodified secretion in 3D (CCL2, CCL3) others are increased (CCL20) or others even strongly reduced (CCL19) compared to 2D (Supplemental Figure 5A). We also find that TNF-α is not modulated contrary to IL-6 and we demonstrate that integrins β_1, β_2 but also β_3 are involved in this increased expression in 3D. The implication of integrin β_3 is particularly interesting as it is known to be an IL-1β receptor [33]. Accordingly, we find an IL-1β signature in 3D macrophages in response to IFNγ/LPS (Figure 6B). We then demonstrate that this IL-1β signature is under the control of the NLRP3 inflammasome in an integrin independent mechanism (Figure 6 D, 6E, 6F). As the growing field of biomaterial research is progressively moving from biocompatible “immunoevasive” materials to “immune-modulating” materials, the implication of inflammasome in macrophage response to biomaterials is of outstanding interest [44]. As we have demonstrated the 3D collagen environment is able to prime macrophages NLRP3 inflammasome and increase the sensivity of these cells to a second signal driving the secretion of huge amount of IL-1β. The mechanism by which the inflammasome of macrophages is primed in 3D is not known but we have shown that the direct implication of integrin activation through the extracellular matrix is unlikely.

We focus our attention on collagen induced immuno-modulation of macrophages, as collagen is the most abundant extracellular matrix (ECM) component in humans. Collagen has also been involved in various pathological contexts. During cancer progression, the ECM is constantly remodelled mainly due to collagen degradation, deposition or cross-linking leading to the stiffening of the tissue [45]. In that particular context, collagen appears as a regulator for tumor associated immune cells such as macrophages. Type I collagen has been reported as being able to reduce macrophage cytotoxicity against cancerous cells [46]. The usual understanding of this result being that collagen is able to inhibit M1 polarization. Our results moderate and complete this interpretation, as in 3D collagen type I environment we found that the M1 driven signalling molecular pathway was responsive and we observe no collagen type I induced inhibition of human monocyte commitment to differentiate toward M1 macrophages. Meanwhile, we found an increase secretion of IL-6 associated with the 3D collagen scaffold. IL-6 has been demonstrated to inhibit maturation of dendritic cells and by the way to inhibit the anti-tumor immune response [47,48]. We also found that IL-1β is increased in 3D collagen setting and this cytokine has been implied in tumor angiogenesis [49]. Along with the demonstration that class II HLA molecules are not differentially expressed in 3D, our study highlights the reappraisal of the immunomodulation induced in 3D by collagen, revealing that it is not related to a global inhibition of the commitment to produce M1 macrophages. These results shade lights on the complexity of the macrophages involvement around tumor nests where they are able to promote or inhibit tumor progression depending on the cellular environment context taking into account the ECM composition [50].

5. Conclusions

In this study we demonstrate that in a 3D collagen type I context, some markers, used in the classification of macrophage polarizations, should be reassessed. The resulting list of markers could be organized according to a functional subdivision and used to complete our present knowledge of macrophage's biology (Figure 7). These results are of a particular

interest in the field of immune-oncology where the macrophage involvement and targeting need a thoughtful understanding of cellular environmental clues leading to various activation states.

Author contributions

MC, MM, AM performed experiments and analyzed data. AM conceived the project, designed experiments, supervised the study, raised funding and wrote the paper.

Competing interest

The authors declare no financial and non-financial competing interests

Acknowledgements

AM is supported by the ATIP/Avenir Young group leader program (Inserm). This work was supported by La ligue nationale contre le cancer and by la Fondation ARC pour la recherche sur le cancer. We thank Amiram Ariel for discussion. We thank Alexei Grichine from the cell imaging facility of the Institute for Advanced Studies for his technical help. The confocal microscopy facility was partly funded by the Association for Research on Cancer, French Ministry “Enseignement Superieure et Recherche” and the Rhone-Alpes region (Contrat de projets Etat–Région 2007-2013 “Exploration du vivant, Imagerie biomedicale”). We thank Michèle El-Atifi for her technical help in RNA samples preparation.

Data availability

The raw data required to reproduce these findings are available to download from www.proteomexchange.org/ and https://www.ncbi.nlm.nih.gov/geo. The processed data required to reproduce these findings are available to download from www.proteomexchange.org/ and https://www.ncbi.nlm.nih.gov/geo. The mass spectrometry proteomics data have been deposited to the ProteomeXchange Consortium via the PRIDE

partner repository with the dataset identifier PXD012147. RNA sequencing data are deposited in the NCBI Gene Expression Omnibus under accession number: GSE124738.

References

[1] Y. Okabe, R. Medzhitov, Tissue biology perspective on macrophages, Nat. Immunol. 17 (2016) 9–17. doi:10.1038/ni.3320.

[2] A. Sica, A. Mantovani, Macrophage plasticity and polarization: in vivo veritas, J. Clin. Invest. 122 (2012) 787–795. doi:10.1172/JCI59643.

[3] F.O. Martinez, S. Gordon, M. Locati, A. Mantovani, Transcriptional profiling of the human monocyte-to-macrophage differentiation and polarization: new molecules and patterns of gene expression, J. Immunol. Baltim. Md 1950. 177 (2006) 7303–7311.

[4] P.J. Murray, J.E. Allen, S.K. Biswas, E.A. Fisher, D.W. Gilroy, S. Goerdt, S. Gordon, J.A. Hamilton, L.B. Ivashkiv, T. Lawrence, M. Locati, A. Mantovani, F.O. Martinez, J.-L. Mege, D.M. Mosser, G. Natoli, J.P. Saeij, J.L. Schultze, K.A. Shirey, A. Sica, J. Suttles, I. Udalova, J.A. van Ginderachter, S.N. Vogel, T.A. Wynn, Macrophage activation and polarization: nomenclature and experimental guidelines, Immunity. 41 (2014) 14–20. doi:10.1016/j.immuni.2014.06.008.

[5] S. Gordon, F.O. Martinez, Alternative activation of macrophages: mechanism and functions, Immunity. 32 (2010) 593–604. doi:10.1016/j.immuni.2010.05.007.

[6] F.Y. McWhorter, C.T. Davis, W.F. Liu, Physical and mechanical regulation of macrophage phenotype and function, Cell. Mol. Life Sci. CMLS. 72 (2015) 1303–1316. doi:10.1007/s00018-014-1796-8.

[7] A. Singh, N.A. Peppas, Hydrogels and scaffolds for immunomodulation, Adv. Mater. Deerfield Beach Fla. 26 (2014) 6530–6541. doi:10.1002/adma.201402105.

[8] R. Sridharan, A.R. Cameron, D.J. Kelly, C.J. Kearney, F.J. O'Brien, Biomaterial based modulation of macrophage polarization: a review and suggested design principles, Mater. Today. 18 (2015) 313–325. doi:10.1016/j.mattod.2015.01.019.

[9] P.L. Graney, E.B. Lurier, K.L. Spiller, Biomaterials and Bioactive Factor Delivery Systems for the Control of Macrophage Activation in Regenerative Medicine, ACS Biomater. Sci. Eng. 4 (2018) 1137–1148. doi:10.1021/acsbiomaterials.6b00747.

591 [10] N.L. Springer, C. Fischbach, Biomaterials approaches to modeling macrophage-extracellular
592 matrix interactions in the tumor microenvironment, Curr. Opin. Biotechnol. 40 (2016) 16–23.
593 doi:10.1016/j.copbio.2016.02.003.
594 [11] F.Y. McWhorter, T. Wang, P. Nguyen, T. Chung, W.F. Liu, Modulation of macrophage
595 phenotype by cell shape, Proc. Natl. Acad. Sci. U. S. A. 110 (2013) 17253–17258.
596 doi:10.1073/pnas.1308887110.
597 [12] A.K. Blakney, M.D. Swartzlander, S.J. Bryant, The effects of substrate stiffness on the in vitro
598 activation of macrophages and in vivo host response to poly(ethylene glycol)-based hydrogels,
599 J. Biomed. Mater. Res. A. 100 (2012) 1375–1386. doi:10.1002/jbm.a.34104.
600 [13] E.F. Irwin, K. Saha, M. Rosenbluth, L.J. Gamble, D.G. Castner, K.E. Healy, Modulus-dependent
601 macrophage adhesion and behavior, J. Biomater. Sci. Polym. Ed. 19 (2008) 1363–1382.
602 doi:10.1163/156856208786052407.
603 [14] N.R. Patel, M. Bole, C. Chen, C.C. Hardin, A.T. Kho, J. Mih, L. Deng, J. Butler, D. Tschumperlin,
604 J.J. Fredberg, R. Krishnan, H. Koziel, Cell elasticity determines macrophage function, PloS One.
605 7 (2012) e41024. doi:10.1371/journal.pone.0041024.
606 [15] M.L. Previtera, A. Sengupta, Substrate Stiffness Regulates Proinflammatory Mediator
607 Production through TLR4 Activity in Macrophages, PloS One. 10 (2015) e0145813.
608 doi:10.1371/journal.pone.0145813.
609 [16] S. Franz, F. Allenstein, J. Kajahn, I. Forstreuter, V. Hintze, S. Möller, J.C. Simon, Artificial
610 extracellular matrices composed of collagen I and high-sulfated hyaluronan promote
611 phenotypic and functional modulation of human pro-inflammatory M1 macrophages, Acta
612 Biomater. 9 (2013) 5621–5629. doi:10.1016/j.actbio.2012.11.016.
613 [17] M. Friedemann, L. Kalbitzer, S. Franz, S. Moeller, M. Schnabelrauch, J.-C. Simon, T. Pompe, K.
614 Franke, Instructing Human Macrophage Polarization by Stiffness and Glycosaminoglycan
615 Functionalization in 3D Collagen Networks, Adv. Healthc. Mater. 6 (2017) 1600967.
616 doi:10.1002/adhm.201600967.
617 [18] J.J. Green, J.H. Elisseeff, Mimicking biological functionality with polymers for biomedical
618 applications, Nature. 540 (2016) 386–394. doi:10.1038/nature21005.
619 [19] D. Kim, G. Pertea, C. Trapnell, H. Pimentel, R. Kelley, S.L. Salzberg, TopHat2: accurate alignment
620 of transcriptomes in the presence of insertions, deletions and gene fusions, Genome Biol. 14
621 (2013) R36. doi:10.1186/gb-2013-14-4-r36.
622 [20] S. Anders, P.T. Pyl, W. Huber, HTSeq--a Python framework to work with high-throughput
623 sequencing data, Bioinforma. Oxf. Engl. 31 (2015) 166–169.
624 doi:10.1093/bioinformatics/btu638.
625 [21] S. Anders, W. Huber, Differential expression analysis for sequence count data, Genome Biol. 11
626 (2010) R106. doi:10.1186/gb-2010-11-10-r106.
627 [22] L. Wang, S. Wang, W. Li, RSeQC: quality control of RNA-seq experiments, Bioinforma. Oxf. Engl.
628 28 (2012) 2184–2185. doi:10.1093/bioinformatics/bts356.
629 [23] M. Court, G. Petre, M.E. Atifi, A. Millet, Proteomic Signature Reveals Modulation of Human
630 Macrophage Polarization and Functions Under Differing Environmental Oxygen Conditions,
631 Mol. Cell. Proteomics MCP. 16 (2017) 2153–2168. doi:10.1074/mcp.RA117.000082.
632 [24] J. Cox, M.Y. Hein, C.A. Luber, I. Paron, N. Nagaraj, M. Mann, Accurate proteome-wide label-free
633 quantification by delayed normalization and maximal peptide ratio extraction, termed MaxLFQ,
634 Mol. Cell. Proteomics MCP. 13 (2014) 2513–2526. doi:10.1074/mcp.M113.031591.
635 [25] J. Cox, N. Neuhauser, A. Michalski, R.A. Scheltema, J.V. Olsen, M. Mann, Andromeda: a peptide
636 search engine integrated into the MaxQuant environment, J. Proteome Res. 10 (2011) 1794–
637 1805. doi:10.1021/pr101065j.
638 [26] J.E. Sader, R. Borgani, C.T. Gibson, D.B. Haviland, M.J. Higgins, J.I. Kilpatrick, J. Lu, P. Mulvaney,
639 C.J. Shearer, A.D. Slattery, P.-A. Thorén, J. Tran, H. Zhang, H. Zhang, T. Zheng, A virtual
640 instrument to standardise the calibration of atomic force microscope cantilevers, Rev. Sci.
641 Instrum. 87 (2016) 093711. doi:10.1063/1.4962866.

[27] P. Hermanowicz, M. Sarna, K. Burda, H. Gabryś, AtomicJ: an open source software for analysis of force curves, Rev. Sci. Instrum. 85 (2014) 063703. doi:10.1063/1.4881683.
[28] A.V. Villarino, Y. Kanno, J.J. O'Shea, Mechanisms and consequences of Jak-STAT signaling in the immune system, Nat. Immunol. 18 (2017) 374–384. doi:10.1038/ni.3691.
[29] J.E. Darnell, I.M. Kerr, G.R. Stark, Jak-STAT pathways and transcriptional activation in response to IFNs and other extracellular signaling proteins, Science. 264 (1994) 1415–1421.
[30] M.F. Krummel, J.N. Mahale, L.F.K. Uhl, E.A. Hardison, A.M. Mujal, J.M. Mazet, R.J. Weber, Z.J. Gartner, A. Gérard, Paracrine costimulation of IFN-γ signaling by integrins modulates CD8 T cell differentiation, Proc. Natl. Acad. Sci. U. S. A. 115 (2018) 11585–11590. doi:10.1073/pnas.1804556115.
[31] D.J. Conrad, M. Lu, Regulation of human 12/15-lipoxygenase by Stat6-dependent transcription, Am. J. Respir. Cell Mol. Biol. 22 (2000) 226–234.
[32] V.P. Yakubenko, A. Bhattacharjee, E. Pluskota, M.K. Cathcart, $\alpha M\beta_2$ integrin activation prevents alternative activation of human and murine macrophages and impedes foam cell formation, Circ. Res. 108 (2011) 544–554. doi:10.1161/CIRCRESAHA.110.231803.
[33] Y.K. Takada, J. Yu, M. Fujita, J. Saegusa, C.-Y. Wu, Y. Takada, Direct binding to integrins and loss of disulfide linkage in interleukin-1β (IL-1β) are involved in the agonistic action of IL-1β, J. Biol. Chem. 292 (2017) 20067–20075. doi:10.1074/jbc.M117.818302.
[34] C.M. Cahill, J.T. Rogers, Interleukin (IL) 1beta induction of IL-6 is mediated by a novel phosphatidylinositol 3-kinase-dependent AKT/IkappaB kinase alpha pathway targeting activator protein-1, J. Biol. Chem. 283 (2008) 25900–25912. doi:10.1074/jbc.M707692200.
[35] P.J. Murray, Macrophage Polarization, Annu. Rev. Physiol. 79 (2017) 541–566. doi:10.1146/annurev-physiol-022516-034339.
[36] R. Pacifici, J. Roman, R. Kimble, R. Civitelli, C.M. Brownfield, C. Bizzarri, Ligand binding to monocyte alpha 5 beta 1 integrin activates the alpha 2 beta 1 receptor via the alpha 5 subunit cytoplasmic domain and protein kinase C, J. Immunol. Baltim. Md 1950. 153 (1994) 2222–2233.
[37] T.H. Lin, C. Rosales, K. Mondal, J.B. Bolen, S. Haskill, R.L. Juliano, Integrin-mediated tyrosine phosphorylation and cytokine message induction in monocytic cells. A possible signaling role for the Syk tyrosine kinase, J. Biol. Chem. 270 (1995) 16189–16197.
[38] B.-H. Cha, S.R. Shin, J. Leijten, Y.-C. Li, S. Singh, J.C. Liu, N. Annabi, R. Abdi, M.R. Dokmeci, N.E. Vrana, A.M. Ghaemmaghami, A. Khademhosseini, Integrin-Mediated Interactions Control Macrophage Polarization in 3D Hydrogels, Adv. Healthc. Mater. 6 (2017). doi:10.1002/adhm.201700289.
[39] R. Garnotel, L. Rittié, S. Poitevin, J.C. Monboisse, P. Nguyen, G. Potron, F.X. Maquart, A. Randoux, P. Gillery, Human blood monocytes interact with type I collagen through alpha x beta 2 integrin (CD11c-CD18, gp150-95), J. Immunol. Baltim. Md 1950. 164 (2000) 5928–5934.
[40] N.K. Singh, G.N. Rao, Emerging role of 12/15-Lipoxygenase (ALOX15) in human pathologies, Prog. Lipid Res. (2018). doi:10.1016/j.plipres.2018.11.001.
[41] F.O. Martinez, L. Helming, R. Milde, A. Varin, B.N. Melgert, C. Draijer, B. Thomas, M. Fabbri, A. Crawshaw, L.P. Ho, N.H. Ten Hacken, V. Cobos Jiménez, N.A. Kootstra, J. Hamann, D.R. Greaves, M. Locati, A. Mantovani, S. Gordon, Genetic programs expressed in resting and IL-4 alternatively activated mouse and human macrophages: similarities and differences, Blood. 121 (2013) e57-69. doi:10.1182/blood-2012-06-436212.
[42] D. Wang, K.M. Bratlie, Influence of Polymer Chemistry on Cytokine Secretion from Polarized Macrophages, ACS Biomater. Sci. Eng. 1 (2015) 166–174. doi:10.1021/ab5001063.
[43] D.Y.S. Chau, R.J. Collighan, E.A.M. Verderio, V.L. Addy, M. Griffin, The cellular response to transglutaminase-cross-linked collagen, Biomaterials. 26 (2005) 6518–6529. doi:10.1016/j.biomaterials.2005.04.017.
[44] D.P. Vasconcelos, A.P. Águas, M.A. Barbosa, P. Pelegrín, J.N. Barbosa, The inflammasome in host response to biomaterials: Bridging inflammation and tissue regeneration, Acta Biomater. 83 (2019) 1–12. doi:10.1016/j.actbio.2018.09.056.

[45] M. Fang, J. Yuan, C. Peng, Y. Li, Collagen as a double-edged sword in tumor progression, Tumour Biol. J. Int. Soc. Oncodevelopmental Biol. Med. 35 (2014) 2871–2882. doi:10.1007/s13277-013-1511-7.
[46] G. Kaplan, In vitro differentiation of human monocytes. Monocytes cultured on glass are cytotoxic to tumor cells but monocytes cultured on collagen are not, J. Exp. Med. 157 (1983) 2061–2072.
[47] S. Hegde, J. Pahne, S. Smola-Hess, Novel immunosuppressive properties of interleukin-6 in dendritic cells: inhibition of NF-κB binding activity and CCR7 expression, FASEB J. 18 (2004) 1439–1441. doi:10.1096/fj.03-0969fje.
[48] S.-J. Park, T. Nakagawa, H. Kitamura, T. Atsumi, H. Kamon, S. Sawa, D. Kamimura, N. Ueda, Y. Iwakura, K. Ishihara, M. Murakami, T. Hirano, IL-6 Regulates In Vivo Dendritic Cell Differentiation through STAT3 Activation, J. Immunol. 173 (2004) 3844–3854. doi:10.4049/jimmunol.173.6.3844.
[49] E. Voronov, D.S. Shouval, Y. Krelin, E. Cagnano, D. Benharroch, Y. Iwakura, C.A. Dinarello, R.N. Apte, IL-1 is required for tumor invasiveness and angiogenesis, Proc. Natl. Acad. Sci. U. S. A. 100 (2003) 2645–2650. doi:10.1073/pnas.0437939100.
[50] M. Yang, D. McKay, J.W. Pollard, C.E. Lewis, Diverse Functions of Macrophages in Different Tumor Microenvironments, Cancer Res. 78 (2018) 5492–5503. doi:10.1158/0008-5472.CAN-18-1367.

Figure Legends

Figure 1 Transcriptomic analysis of human macrophages in 2D and 3D environment.

(A) Human monocytes are directly differentiated with M-CSF in their respective 2D or 3D environment for 6 days prior to polarisation toward M1 (IFNγ/LPS) or M2 (IL-4/IL-13). (B) Phase contrast imaging of M1 and M2 macrophages on collagen coated surfaces (2D) and in collagen gels (3D). Scale bar = 50 µm. (C) Quantification of the size of cells using their major axis based on phase contrast imaging. Aspect ratio defined by the ratio between major axis (a) and minor axis (b) is also quantified. Tukey's multiple comparison test was used. (ns=non significant, * $p<0.05$, ** $p<0.01$, *** $p<0.001$, **** $p<0.0001$). (D) Principal component analysis of gene expression (RNAseq) in macrophages showing that the first component (43.8%) resolves the M1 and M2 dichotomy and the second (21.5%) the 2D/3D one. (E) Volcano-plot representation of M1/M2 differential gene expression in 2D (left panel) and 3D (right panel). Fold change threshold was set at 2 and p-value is calculated using a

paired Welch t test with Benjamini-Hochberg correction, the threshold is set at 0.05. 9141 genes are analysed in 2D and 9733 in 3D using a filter for FPKM >0.5.

Figure 2 STAT1 phosphorylation under IFNγ/LPS polarisation is increased in 3D under an integrin β_2 mechanism.

(A) Human macrophages express significant level of STAT1α/β when stimulated by IFNγ/LPS as revealed by western blotting. The serine 727 phosphorylation is significantly increased in 3D M1 macrophages. (Tukey's multiple comparison test, three independent experiments, ** p<0.01, ****p<0.001). (B) STAT1 serine 727 phosphorylation and STAT1α/β expression in 3D M1 macrophages exposed to various blocking antibodies targeting integrins. Blocking of integrin β2 decrease significantly the level of phosphorylation of STAT1 without modifying the level of the protein expression. (Dunnett's multiple comparison test toward the control condition, three independent experiments, ** p<0.01). All level proteins expression are normalized to β-actin level. Values in all panels are mean +/- SEM.

Figure 3 ALOX15 expression is repressed by an integrin β_2 mechanism in 3D M2 macrophages associated with an increase of STAT6 phosphorylation and upregulation of transglutaminase 2.

(A) Immunoblotting of STAT6 and pSTAT6^{tyr641} demonstrating the increase of phosphorylation in 3D under the IL4/IL13 stimulation. Normalisation is performed with β-actin (Tukey's multiple comparison test, three independent experiments, * p<0.05, ** p<0.01). (B) Immunoblotting of ALOX15 and TGM2 showing the downregulation of ALOX15 in 3D and the increase of expression of TGM2. Normalisation is performed toward β-actin (Tukey's multiple comparison test, three independent experiments, ** p<0.01, *** p<0.001). (C) RNA level expression of ALOX15 and TGM2 from RNAseq analysis expressed in FPKM (Fragment per per kilobase of exon model per million reads mapped; Tukey's multiple comparison test, three independent experiments, * <0.05, ** p<0.01, *** p<0.001, **** p<0.0001). (D) Immunoblotting of CD206, ALOX15, STAT6, TGM2 and β-actin on M2

753 macrophages in 2D and 3D. Blocking antibodies against integrins β_1 and β_2 are added to 3D
754 macrophages. Representative results from three independent experiments. Values in all
755 panels are mean +/- SEM.

756 Figure 4 Class II HLA expression is no longer a key element of the M1/M2 dichotomy in 3D.

757 (A) Gene Ontology (GO) of Biological Processes (BP) analysis for up-regulated mRNA in
758 M2 human macrophages compared to their M1 counterpart in 2D and in 3D. p-value was
759 adjusted using the Benjamini-Hochberg procedure (B) Cell plot representation of the
760 expression of all HLA genes found in our RNAseq analysis. We have separated these
761 molecules according to major histocompatibility complex class. Color scale represents z-
762 score of FPKM reads. (C) Cell plot representation of the expression of all HLA proteins
763 identified and quantified in our proteomic study. We have separated these molecules
764 according the major histocompatibility complex class. Color scale represents z-score of LFQ
765 intensity. UniProt knowledgebase entries are indicated.

766 Figure 5 Macrophages secretome is modulated by 3D. M1 are prone to secrete more IL-6 in
767 an integrin dependent mechanism and present an inverted CCL19/CCL20 ratio.

768 (A) Cell plot representation of the expression of cytokines, chemokines and receptors found
769 in our RNAseq analysis. We have performed M1/M2 ratio and set the threshold for fold
770 change at 4, the statistical significance was assessed by a paired Welch t test with a
771 Benjamini-Hochberg correction. Genes were classified according their shared pattern in 2D
772 and 3D. (B) Supernatant of M1 macrophages were collected and analysed on chemokine
773 array membranes which confirm at the protein level the inverse regulation of CCL19 and
774 CCL20 between 2D and 3D. Upper panel 2D and lower panel 3D. Result representative of
775 three independent experiments. (C) ELISA quantification of CCL19 and CCL20 in
776 supernatants of M1 macrophages confirming the inversion of the CCL19/CCL20 ratio
777 between the 2D and 3D environment. (Tukey's multiple comparison test, four independent
778 experiments, * $p<0.05$, **** $p<0.001$). (D) ELISA quantification of IL-6 secretion of M1

779 macrophages showing the increase in 3D (Left panel, Paired t-test, four independent
780 experiments, * $p<0.05$). Blocking antibodies against integrins demonstrate that β_2, α_2, β_1 and
781 β_3 are involved in this process (Dunnett's multiple comparison test toward the control
782 condition, four independent experiments, * $p<0.05$, ** $p<0.01$). (E) ELISA quantification of
783 TNF-α secretion of M1 macrophages showing no difference between 2D and 3D (Left panel,
784 Paired t-test, four independent experiments). Blocking antibodies against integrins show no
785 modulation of TNF-α secretion (Dunnett's multiple comparison test toward the control
786 condition, four independent experiments). Values in all panels are mean +/- SEM.

787 Figure 6 The 3D environment drives an IL-1β secretion in response to IFNγ/LPS in a NLRP3
788 inflammasome dependent pathway in an integrin-independent mechanism.

789 (A) mRNA levels of CASP1 genes expression predominantly expressed in M1 and IL1B
790 expression predominantly expressed in M1 3D macrophages (mRNA levels are expressed in
791 FPKM=Fragment per per kilobase of exon model per million reads mapped). (B) ELISA
792 quantification of IL-1β secretion confirming the specific expression in M1 3D human
793 macrophages. (Tukey's multiple comparison test, five independent experiments, *$p<0.05$).
794 (C) Immunoblotting of pro-CASP1 in macrophages in 2D and 3D exposed to IFNγ and LPS
795 in medium without serum during 3 hours. Representative result from three independent
796 experiments. β-actin is used as control loading. (D) ELISA quantification of IL-1β secretion
797 showing the inhibitory effect of MCC950, a specific inhibitor of NLRP3 inflammasome, in M1
798 macrophages (Tukey's multiple comparison test, five independent experiments, ***
799 $p<0.001$). (E) ELISA quantification of IL-1β secretion after 1 hour of ATP stimulation on
800 previously primed macrophages by LPS at 1 ng/mL during 16 hours (Tukey's multiple
801 comparison test, four independent experiments, * $p<0.05$). (F) ELISA quantification of IL-1β
802 secretion in M1 3D macrophages under the blocking of various integrins showing no
803 inhibition of the release (Dunnett's multiple comparison test toward the control condition, five
804 independent experiments, no statistical significant differences were found). Values in all
805 panels are mean +/- SEM.

Figure 7 Reassessment of specific markers of human macrophages polarization in 3D.

We have represented specific markers for human macrophage polarisations. Markers that were already known (Murray et al, 2014) and confirmed in our study are represented in black. New markers that are able to distinguish M1 and M2 in a 2D or a 3D environment that have been found in our study are represented in red. Capital letters represent protein and italic capital letters genes. When genes and proteins are identified, we represent proteins alone.

Supplementary Data

Supplemental Figure 1 Differentiated human macrophages are distributed in 3D in collagen gel.

Confocal imaging experiments were performed using a LSM710 NLO (Carl Zeiss) laser scanning. Macrophages were stained with Hoechst (nucleus staining) and Phalloidin Alexa488 (actin staining). Z-stack over 350 µm was imaged with the step of 2 µm demonstrating the 3D distribution of macrophages.

Supplemental Figure 2 Gene signature of M1/M2 macrophages in 2D and 3D environment.

(A) Cell plot representation of specifically expressed genes in M1 macrophages for 2D and 3D conditions. Genes were grouped according functional annotation. (B) Cell plot representation of specifically expressed genes in M2 macrophages for 2D and 3D

conditions. Genes are grouped according functional annotation. Quantification is performed using the z-score of the FPKM reads. Genes are selected if the fold change is greater than 2 in one condition and not the other (Statistical significance was evaluated with Welch paired t test with Benjamini-Hochberg correction for multiple comparison; p-adjusted-value <0.05). Results are obtained from three independent experiments.

Supplemental Figure 3 Integrin expression in human macrophages

mRNA expression level of ITGB1 (Integrin β_1), ITGB2 (Integrin β_2), ITGB3 (Integrin β_3), ITGAL (integrin CD11a), ITGAM (Integrin CD11b) and ITGAX (Integrin CD11c) from the RNAseq analysis. Results from three independent experiments. mRNA levels are expressed in FPKM (Fragment per per kilobase of exon model per million reads mapped).

Supplemental Figure 4 Protein signature of M1/M2 macrophages in 2D and 3D environment

(A) Cell plot representation of specifically expressed proteins in M1 macrophages for 2D and 3D conditions. Proteins were grouped according functional annotation. (B) Cell plot representation of specifically expressed proteins in M2 macrophages for 2D and 3D conditions. Proteins are grouped according functional annotation. Quantification is performed using the z-score of the LFQ. Proteins are selected if the fold change is greater than 2 in one condition and not the other (Statistical significance was evaluated with Welch paired t test with Benjamini-Hochberg correction for multiple comparison; p-adjusted-value <0.05). Results are obtained from two independent experiments with three analytical replicates.

Supplemental Figure 5 STAT6 phosphorylation in 3D is integrin independent

Immunoblotting of $pSTAT6^{Tyr641}$ is done on M2 macrophages in 2D and 3D with blocking antibodies against integrins. β-Actin is used as a control loading.

Supplemental Figure 6 Secretome of M1 macrophages display an inversed CCL19/CCL20 ratio in 3D in an integrin independent mechanism.

(A) Supernatant of M1 macrophages are collected and analyzed on chemokine array membranes which confirm at the protein level the inverse regulation of CCL19 and CCL20 between 2D and 3D. Upper panel 2D and lower panel 3D. This essay also confirms the specificity of this ratio as other chemokines are not significantly modulated. (Paired t-test, n=3, ** $p<0.01$, * $p<0.05$). (B) ELISA quantification of CCL19 demonstrate that 3D secretion in M1 macrophages is not modulated by blocking antibodies directed against integrins. (Dunnett's multiple comparison test toward the control condition, four independent experiments).

Supplemental Figure 7 Macrophages do not significantly modify the elasticity of their surrounding physical environment.

Elasticity of collagen gels containing M1 and M2 macrophages, as well as empty gels, are analyzed with an indentation force-volume measurement with an atomic force microscope. Young modulus of empty gels was found at 235.9 +/- 74.1 Pa (mean +/- SD). Gels containing M1 and M2 gels were measured at 281.7 +/- 162.5 Pa and 307.7 +/- 112 Pa respectively.

Supplemental Table1: Over expressed genes in M1 macrophages shared by 2D and 3D conditions

Supplemental Table 2: Over expressed genes in M2 macrophages shared by 2D and 3D conditions

Supplemental Table 3: Over expressed proteins in M1 macrophages shared by 2D and 3D conditions

Supplemental Table 4: Over expressed proteins in M2 macrophages shared by 2D and 3D conditions

Figure 1

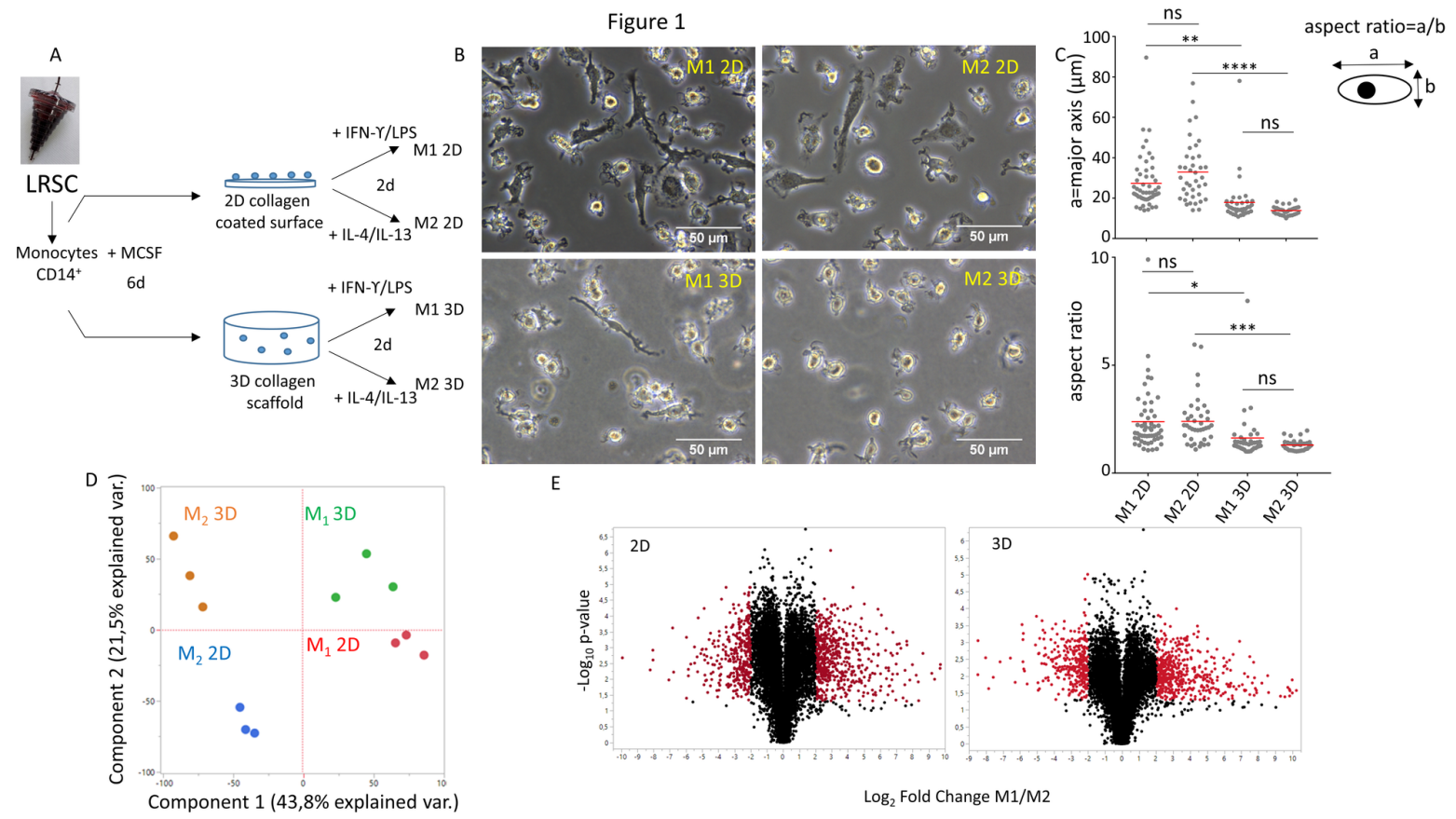
A
LRSC
Monocytes CD14+
+ MCSF
6d
2D collagen coated surface
3D collagen scaffold
+ IFN-γ/LPS
2d
+ IL-4/IL-13
M1 2D
M2 2D
M1 3D
M2 3D
B
M1 2D
M2 2D
M1 3D
M2 3D
50 µm
C
aspect ratio=a/b
a
b
a=major axis (µm)
aspect ratio
ns
**
****
*
***
M1 2D
M2 2D
M1 3D
M2 3D
D
M2 3D
M1 3D
M2 2D
M1 2D
Component 2 (21,5% explained var.)
Component 1 (43,8% explained var.)
E
2D
3D
-Log10 p-value
Log2 Fold Change M1/M2

Figure 2

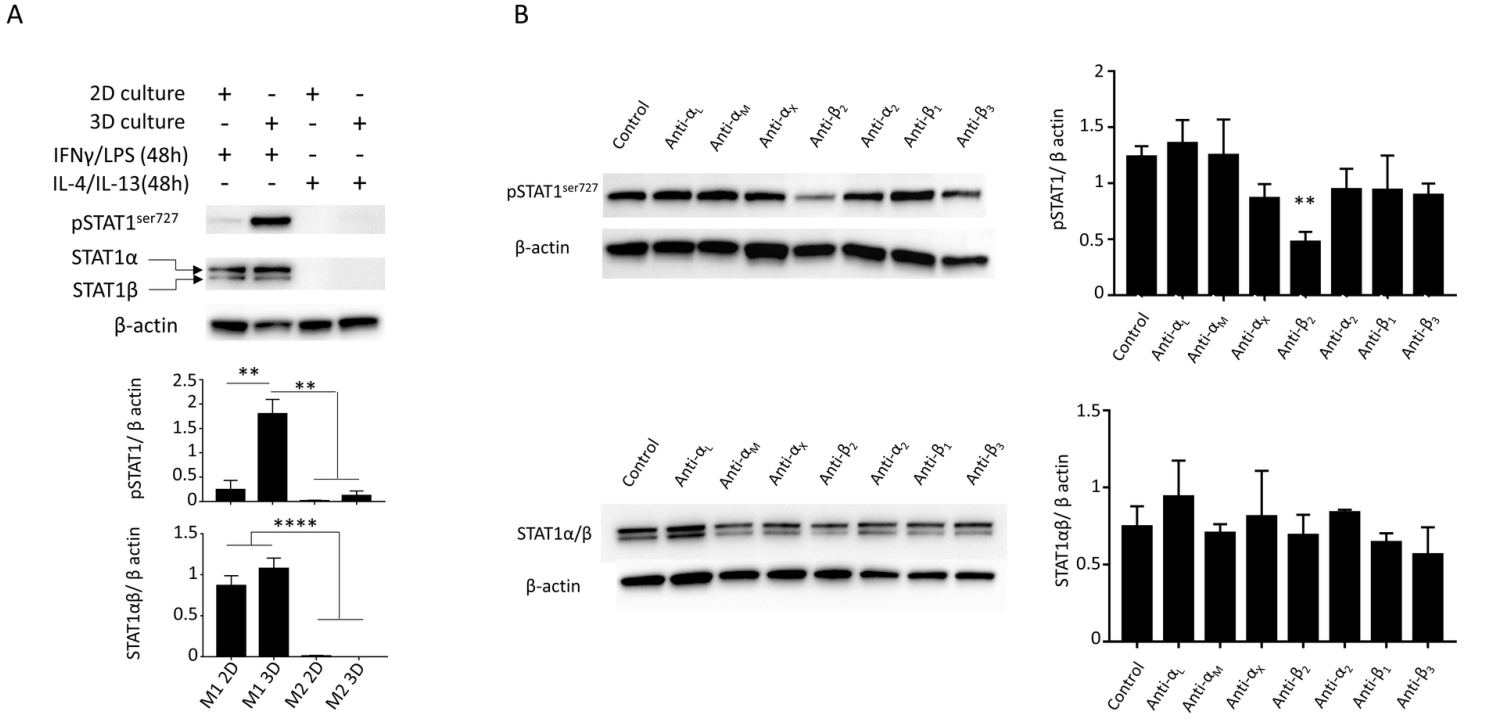
A
2D culture + - + -
3D culture - + - +
IFNγ/LPS (48h) + + - -
IL-4/IL-13(48h) - - + +
pSTAT1ser727
STAT1α
STAT1β
β-actin
pSTAT1/ β actin
STAT1αβ/ β actin
**
**
****
M1 2D
M1 3D
M2 2D
M2 3D
B
Control
Anti-αL
Anti-αM
Anti-αX
Anti-β2
Anti-α2
Anti-β1
Anti-β3
pSTAT1ser727
β-actin
pSTAT1/ β actin
**
STAT1α/β
β-actin
STAT1αβ/ β actin

Figure 3

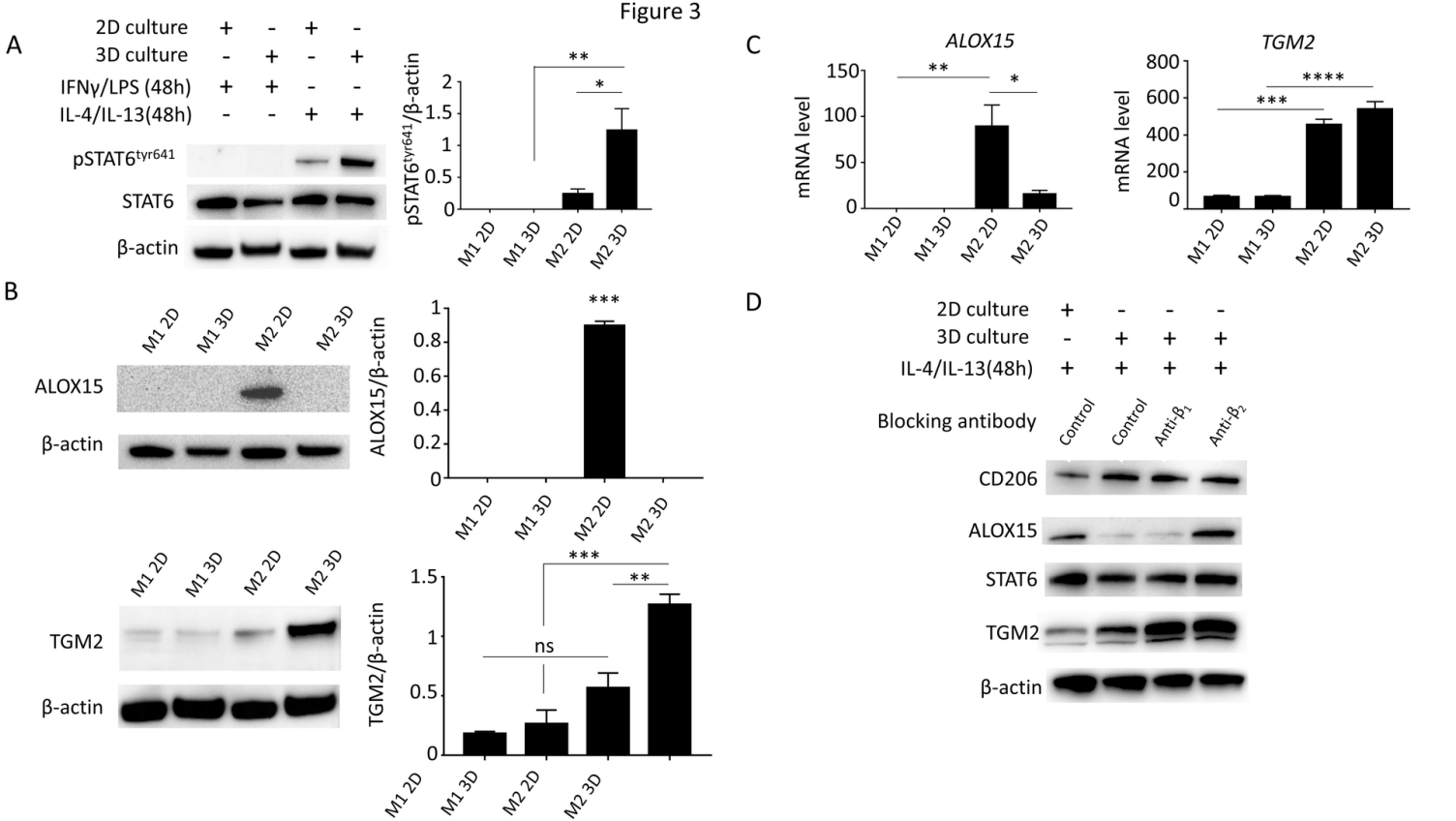
A
2D culture + - + -
3D culture - + - +
IFNγ/LPS (48h) + + - -
IL-4/IL-13(48h) - - + +
pSTAT6tyr641
STAT6
β-actin
pSTAT6tyr641/β-actin
M1 2D
M1 3D
M2 2D
M2 3D
B
ALOX15
β-actin
ALOX15/β-actin
TGM2
β-actin
TGM2/β-actin
ns
C
ALOX15
TGM2
mRNA level
D
2D culture + - - -
3D culture - + + +
IL-4/IL-13(48h) + + + +
Blocking antibody
Control
Control
Anti-β1
Anti-β2
CD206
ALOX15
STAT6
TGM2
β-actin

Figure 4

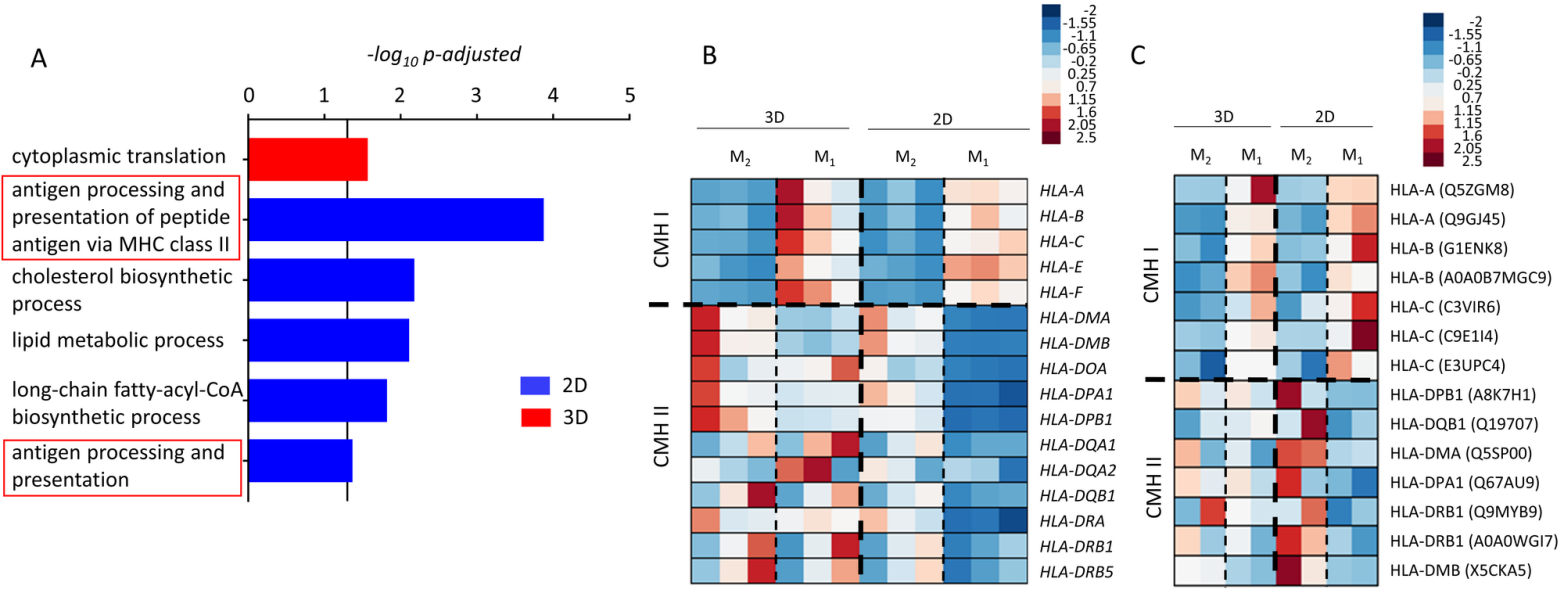
A
-log10 p-adjusted
0
1
2
3
4
5
cytoplasmic translation
antigen processing and presentation of peptide antigen via MHC class II
cholesterol biosynthetic process
lipid metabolic process
long-chain fatty-acyl-CoA biosynthetic process
antigen processing and presentation
2D
3D
B
3D
2D
M2
M1
M2
M1
CMH I
CMH II
HLA-A
HLA-B
HLA-C
HLA-E
HLA-F
HLA-DMA
HLA-DMB
HLA-DOA
HLA-DPA1
HLA-DPB1
HLA-DQA1
HLA-DQA2
HLA-DQB1
HLA-DRA
HLA-DRB1
HLA-DRB5
-2
-1.55
-1.1
-0.65
-0.2
0.25
0.7
1.15
1.6
2.05
2.5
C
3D
2D
M2
M1
M2
M1
CMH I
CMH II
HLA-A (Q5ZGM8)
HLA-A (Q9GJ45)
HLA-B (G1ENK8)
HLA-B (A0A0B7MGC9)
HLA-C (C3VIR6)
HLA-C (C9E1I4)
HLA-C (E3UPC4)
HLA-DPB1 (A8K7H1)
HLA-DQB1 (Q19707)
HLA-DMA (Q5SP00)
HLA-DPA1 (Q67AU9)
HLA-DRB1 (Q9MYB9)
HLA-DRB1 (A0A0WGI7)
HLA-DMB (X5CKA5)
-2
-1.55
-1.1
-0.65
-0.2
0.25
0.7
1.15
1.15
1.6
2.05
2.5

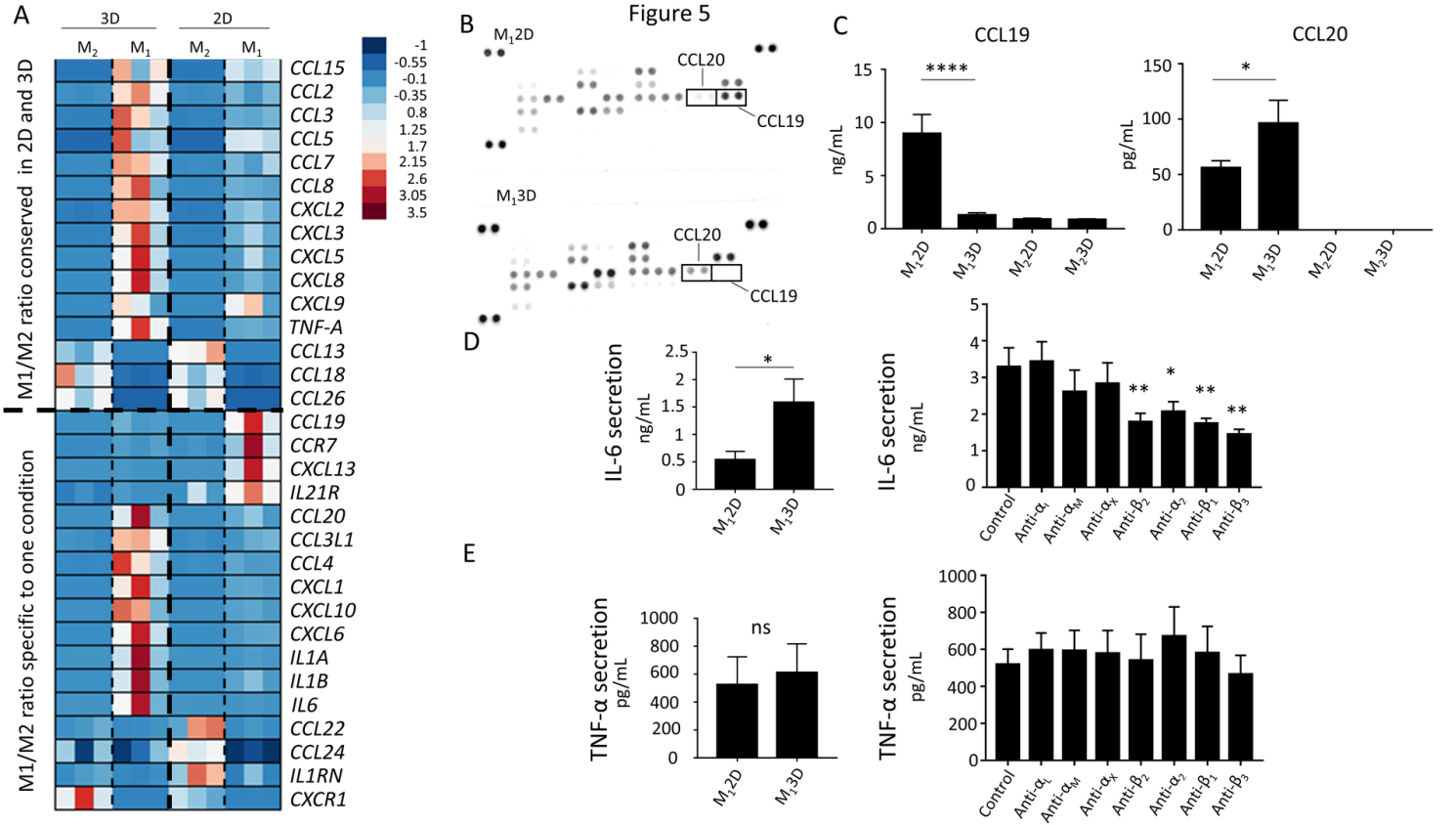
Figure 5
A
3D
2D
M2
M1
M2
M1
M1/M2 ratio conserved in 2D and 3D
M1/M2 ratio specific to one condition
CCL15
CCL2
CCL3
CCL5
CCL7
CCL8
CXCL2
CXCL3
CXCL5
CXCL8
CXCL9
TNF-A
CCL13
CCL18
CCL26
CCL19
CCR7
CXCL13
IL21R
CCL20
CCL3L1
CCL4
CXCL1
CXCL10
CXCL6
IL1A
IL1B
IL6
CCL22
CCL24
IL1RN
CXCR1
-1
-0.55
-0.1
-0.35
0.8
1.25
1.7
2.15
2.6
3.05
3.5
B
M1 2D
CCL20
CCL19
M1 3D
CCL20
CCL19
C
CCL19
ng/mL
****
CCL20
pg/mL
*
M1 2D
M1 3D
M2 2D
M2 3D
D
IL-6 secretion
ng/mL
*
Control
Anti-αL
Anti-αM
Anti-αX
Anti-β2
Anti-α2
Anti-β1
Anti-β3
E
TNF-α secretion
pg/mL
ns

Figure 6

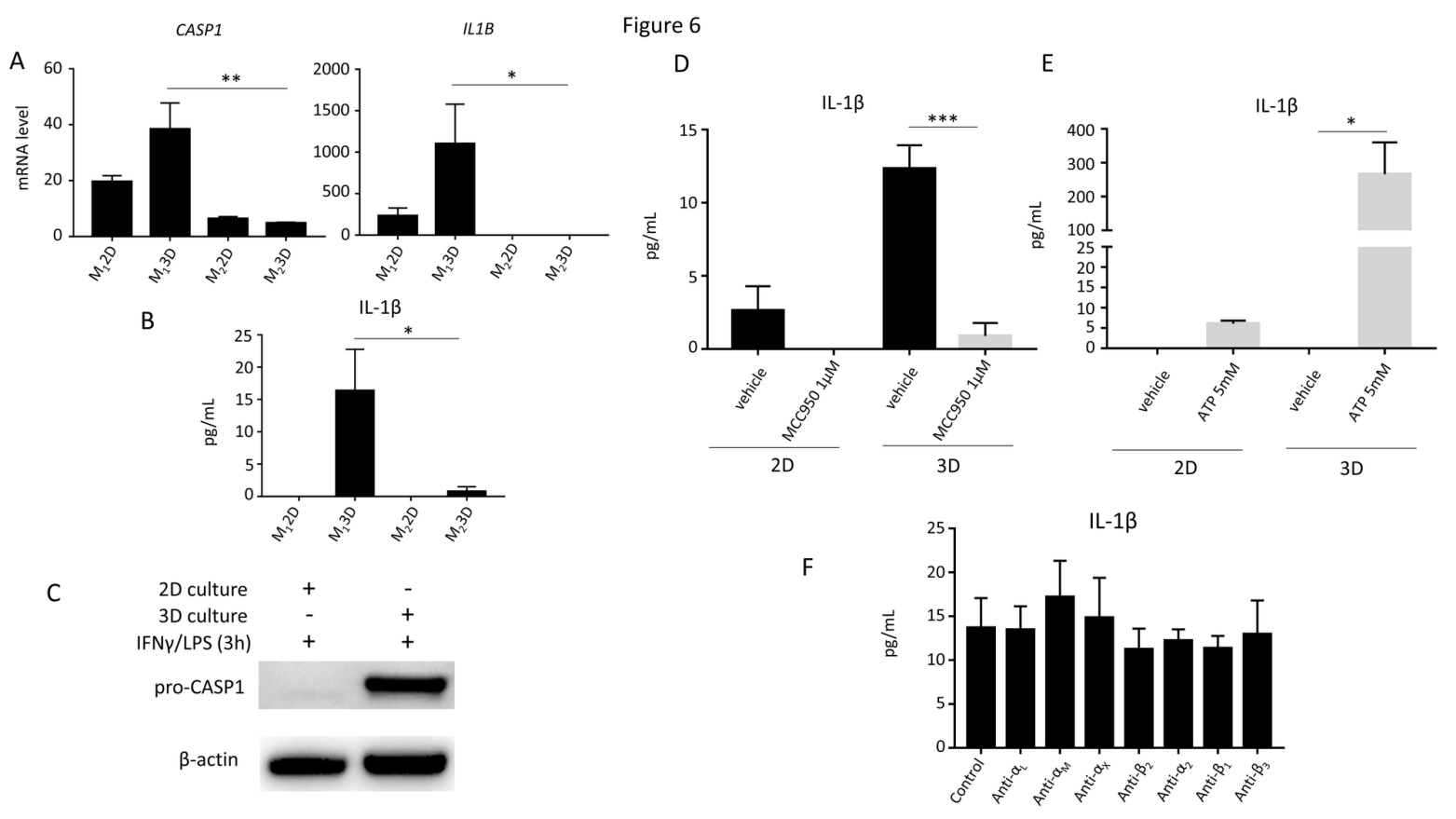
A
CASP1
IL1B
mRNA level
**
*
M1 2D
M1 3D
M2 2D
M2 3D
B
IL-1β
pg/mL
*
C
2D culture + -
3D culture - +
IFNγ/LPS (3h) + +
pro-CASP1
β-actin
D
IL-1β
***
pg/mL
vehicle
MCC950 1μM
2D
3D
E
IL-1β
*
pg/mL
vehicle
ATP 5mM
2D
3D
F
IL-1β
pg/mL
Control
Anti-αL
Anti-αM
Anti-αX
Anti-β2
Anti-α2
Anti-β1
Anti-β3

Figure 7

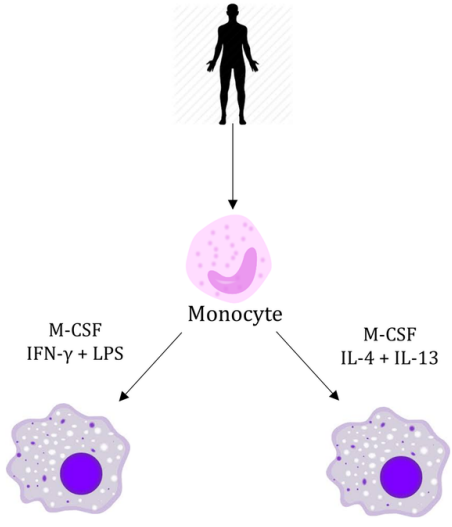

	2D	3D	2D	3D
Transcription factors SOCS proteins	STAT1 *IRF1* pSTAT1	STAT1 *IRF1* pSTAT1++	*SOCS1* pSTAT6	*SOCS1* pSTAT6 ++
Cytokines	TNF-α IL-6	TNF-α IL-6++ IL1β		
Chemokines	CCL5 CXCL8 CXCL9 CXCL10 CCL19++	CCL5 CXCL8 CXCL9 CXCL10 CCL20	*CCL18*	*CCL18*
Scavenger Receptors			MRC1	MRC1
Matrix	MMP9	MMP9	*FN1* *F13A1*	*FN1* *F13A1*
Amino acid metabolism	IDO1 KYNU	IDO1 KYNU		
Others	CD40 GPB1 MHC I *CCR7*	CD40 GPB1 MHC I *ITGB3*	*CD200R* *IL17RB* *TGM2* *ALOX15* MHC II ALOX15	*CD200R* *IL17RB* *TGM2* *ALOX15* TGM2